IEEE Open Journal of
Circuits and Systems

Received 20 March 2021; revised 25 June 2021; accepted 20 July 2021. Date of current version 13 September 2021.

Digital Object Identifier 10.1109/OJCAS.2021.3099869

A Test Setup for the Characterization of Lorentz-Force MEMS Magnetometers

JOSEP MARIA SÁNCHEZ-CHIVA [1,2], JUAN VALLE [2], DANIEL FERNÁNDEZ [3], AND JORDI MADRENAS [2]

[1]Sorbonne Université, CNRS, LIP6, UMR7606, 75252. Paris, France

[2]Department of Electronic Engineering, Universitat Politècnica de Catalunya, 08034 Barcelona, Spain

[3]Institut de Física d'Altes Energies (IFAE-BIST), Edifici Cn. Facultat Ciències Nord, Universitat Autònoma de Barcelona, 08193 Bellaterra, Spain

This article was recommended by Guest Editor L. V. Agostini.

CORRESPONDING AUTHOR: J. M. SÁNCHEZ-CHIVA (e-mail: jose.sanchez_chiva@sorbonne-universite.fr)

This work was supported in part by the Spanish Ministry of Science, Innovation and Universities, the State Research Agency (AEI) under Project RTI2018-099766-B-I00, and in part by the European Social Fund (ESF).

ABSTRACT Lorentz-force MEMS magnetometers are interesting candidates for the replacement of magnetometers in consumer electronics products. Plenty of works in the literature propose MEMS magnetometers, their readout circuits and modulations. However, during the standalone characterization of such MEMS devices, a great variety of instruments and strategies are used, making it very complex to compare results from different works in the literature. For this reason, this article proposes a test setup to characterize Lorentz-force MEMS magnetometers. The proposed setup is based around the use of an impedance analyzer for the driving of voltage and Lorentz-current of the MEMS in-phase and in quadrature, which allows the device Amplitude Modulation and Frequency Modulation characterization. The proposed solution is validated by using the designed circuit to characterize two CMOS-MEMS magnetometers with very different characteristics.

INDEX TERMS Microelectromechanical systems, MEMS, magnetic sensor, magnetometer, Lorentz-force, device characterization, test setup, MEMS measurement.

I. INTRODUCTION

IN THE last decade the technological advances present in consumer electronic products have seen an important boost. A good example of it is the consolidation of smartphone market. Nowadays, *wearables*, activity trackers, and smartwatches are following the same path to commercial success. Moreover, automotive companies are working to offer customers vehicles including Advanced Driver-Assistance Systems (ADAS), and self-driving cars meeting all safety requirements. Such technological advances have been partly possible due to the tremendous improvement in sensor integration: smartphones and *wearables* usually include 9-Degrees-of-Freedom (9-DoF) combos, integrating 3-axis gyroscopes, accelerometers, and magnetometers, while modern electric cars include up to 30 magnetometers per car, a list that is importantly increased by other types of sensors [1], [2].

While accelerometers and gyroscopes are manufactured using MEMS technologies, popular magnetometers are Hall, magnetoresistive (xMR), and Fluxgate sensors [3]. The problem of such magnetometers is the impossibility of integrating them on the same die area of the MEMS sensors, neither on the same die of the electronics. The result of achieving such milestone would mean an important manufacturing cost reduction. In current commercial products, low dimensions are achieved by using System-in-Package: chips consist in a stack of multiple dies containing the MEMS sensors, the magnetic field sensors, and the processing electronics [4].

In order to address the important cost and volume of such products, MEMS magnetometers were proposed as a promising solution that could allow the integration of the magnetometer on the same die of accelerometers and gyroscopes [5]. As a result, the development of Lorentz-force

MEMS magnetometers is currently being developed by several research groups. In a similar direction, CMOS-MEMS [6], [7] devices have been proposed as a solution to not only integrate MEMS magnetometers together with accelerometers and gyroscopes, but to manufacture all these devices on the same electronics die. Following such approach, our research group has developed CMOS-MEMS accelerometers [8], [9], pressure sensors [10], [11], and Lorentz-force magnetometers [12], [13] using the oxide and metal layers available in the Back-End-Of-Line (BEOL) of standard CMOS processes. Like in micro-lithography, the passivation layer is used as a mask that protects the die while a passivation window over the MEMS devices allows the etching acid to etch away the surrounding oxide and release the structures. As a result, the feasibility of manufacturing the MEMS transducers in the same die of the processing electronics has been demonstrated, where the device and the signal processing circuitry are manufactured side by side, which reduce the final product volume, as well as parasitic capacitances.

However, the measurement and characterization of Lorentz-force MEMS magnetometers is challenging. These are resonant sensors that may be driven with a current and voltage biasing, whose phase alignment make the device to work under different modulations. The two most relevant ones are Amplitude Modulation (AM), and Frequency Modulation (FM). In the former, in-phase voltage and current AC drivings are applied at the device's resonance frequency for maximum sensitivity. As a result, the MEMS rotor vibration oscillates proportionally to the magnetic field. Such strategy shows better performance than FM, but requires a more complex demodulation. Moreover, phase deviations make the device to be partly Frequency Modulated, distorting the measurement [14]. FM characterization consist in applying voltage and current drivings that are in quadrature. As a result, the device's resonance frequency changes proportionally to the magnetic field. This strategy is easy to digitize, but has been demonstrated to achieve lower resolution [15], [16].

When it comes to the characterization of devices using AM strategy, a wide variety of measurement setups and sensitivity units may be found in the literature. In this article, a flexible and comprehensive test setup is proposed for the standalone characterization of Lorentz-force MEMS magnetometers in a wide range of driving currents, resonance frequencies and sensor characteristics by using an impedance analyzer. The contribution of this article is multi-fold. First, it proposes a simple yet useful strategy to characterize MEMS magnetometers using an impedance analyzer. As a result, the time consumed by developing measurement setups may be importantly reduced. Second, two sensitivity units are proposed that are not dependent on specific setup characteristics in order to ease comparison with other works on the topic. The sensitivity units are only functions of device parameters and their relationship is disclosed. Third, a comprehensive modification of the presented circuit is proposed for device characterization using frequency modulation.

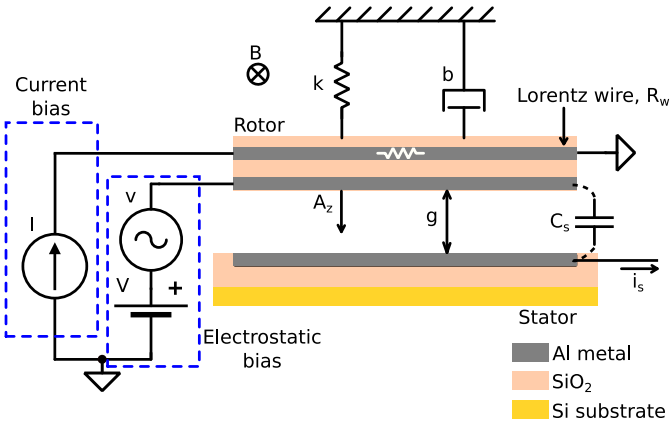

FIGURE 1. Simplified diagram of the MEMS magnetometer with the biasing and the second order electromechanical model included.

The article is organized as follows: first, Section II describes the working principles of Lorentz-force MEMS magnetometers. Next, Section III reviews Lorentz-force MEMS magnetometers characterization strategies. Section IV describes the proposed setup, while its experimental validation is in Section V. The necessary modifications that allow the proposed circuit to drive the MEMS magnetometer under FM operation are proposed in Section VI. Finally, the conclusions are presented in Section VII.

II. WORKING PRINCIPLES OF LORENTZ-FORCE MEMS MAGNETOMETERS

Lorentz-force MEMS magnetometers consist of a movable structure, or rotor, that contains a path for a current to flow. Under the presence of a magnetic field, the current interacts with the field and the structure suffers the so-called Lorentz force. Such force, displaces the rotor, changing its position as a function of the magnetic field intensity. In order to readout such displacement, piezoresistive and capacitive readouts have been proposed, being the latter the most popular. In this work we use capacitive sensing: the two-plate MEMS consists of a movable plate (rotor) and a fixed plate (stator). A simplified diagram is shown in Figure 1.

The Lorentz equation describes the force that a current carrying conductor suffers under the presence of a magnetic field:

$$\vec{F_L} = I\vec{L} \times \vec{B} \tag{1}$$

where I is the current, $\vec{L}$ is the MEMS device rotor length, and $\vec{B}$ is the magnetic field. When the current flows through the MEMS plate, the generated force creates a displacement of the plate. If this driving is done at the resonance frequency f_r, so is the Lorentz force, which multiplies the plate vibration amplitude A_z by the device quality factor Q

$$A_z(f_r) = \frac{Q}{k}(F_L + F_E) \approx \frac{Q}{k}\left(I \cdot L \cdot B + V v \frac{C_s}{g}\right) \tag{2}$$

where k is the spring constant, F_L is the Lorentz force, F_E is the electrostatic force due to the device voltage driving, I is the Lorentz current, L is the device rotor length, B is the sensed magnetic field, V is the DC voltage, v is the AC voltage, C_s is the MEMS device capacitance, and g is the nominal gap. Electrostatic force is a result of driving the magnetometer with a voltage and does not have any dependency neither improve the device performance. In fact, it adds some amount of offset to the readout signal. On the contrary, it is used for a more practical reason: when the device operates in a self-sustained oscillation readout circuit, electrostatic driving allows to maintain oscillation at the device resonance frequency when there is no magnetic field or it is so weak that it is masked by noise [12].

As described by eq. (2), vibration amplitude is amplitude modulated only if I and v terms are in phase as in this situation the electrostatic and Lorentz forces are in phase, adding up and creating a larger rotor oscillation. This is better explained if the second order model of the resonator is observed

$$m\ddot{z} + b\dot{z} + kz = F_E + F_L \tag{3}$$

where m is the rotor mass, b is the damping coefficient, k is the spring constant, F_E and F_L are the electrostatic and Lorentz force respectively, and z, $\dot{z}$ and $\ddot{z}$ are the rotor displacement, velocity and acceleration respectively. If the forces are in phase (this is, voltage and current drivings are in phase), they are both in phase with the rotor velocity $\dot{z}$. Otherwise, when some phase mismatch is present, a proportional fraction of the force is in phase with the rotor displacement z. As a result, the spring coefficient k suffers a variation proportional to the Lorentz force, which changes the devices resonance frequency and, thus, modulates the device frequency. In this situation, eq. (2) does no longer hold as thoroughly explained in [14].

If amplitude modulation is correctly applied, there is an equivalent capacitance variation proportional to such vibration amplitude A_z

$$\Delta C_s = \varepsilon_r \varepsilon_0 A \left(\frac{1}{g} - \frac{1}{g - A_z} \right) \tag{4}$$

where $\varepsilon_r = 1$ is the relative permittivity of air, $\varepsilon_0 \approx 8.854 \cdot 10^{-12} F/m$ is the absolute permittivity, and A is the rotor area. The result of such capacitance variation and voltage driving is the movement of charge $q(t)$ that can be translated to current flowing out the magnetometer capacitance by considering that charge depends on capacitance variation in eq. (4) with $dq(t) = dC_s(t)V$. At the same time, capacitance variation in eq. (4) is a function of the gap variation in eq. (2). By introducing eq. (2) into eq. (4), the expression of charge can be obtained. If the AC voltage v and current I drivings are considered sinusoidal, and the charge is derived as a function of time $dq(t)/dt$, the device output current is obtained:

$$i_s = \frac{dq(t)}{dt} = \frac{\varepsilon_r \varepsilon_0 A Q V \omega_r}{g^2 k} \left(I \cdot L \cdot B + V v \frac{C_s}{g} \right) \tag{5}$$

where $\omega_r = 2\pi f_r$ is the angular resonance frequency. The second part inside parenthesis in eq. (5) is the output current due to the electrostatic driving, which contains no information of the sensed magnetic field. The first half, on the contrary, is the result of the Lorentz force and is the one of interest. Device output current sensitivity as a function of magnetic field may be derived from eq. (5)

$$S_{i_s}(B) = \frac{\partial i_s}{\partial B} = \frac{\varepsilon_r \varepsilon_0 A Q V \omega_r I L}{g^2 k} \tag{6}$$

Such output current is sensed by the impedance analyzer and is translated into admittance units or equivalent. In this article we used the conductance (G). Hence, the higher the magnetic field, the higher is the Lorentz force, which is translated into a greater conductance peak. Device conductance sensitivity can be derived from current in eq. (5) if we consider that $G(f_r) = i_s/v$

$$S_G(B) = \frac{\partial G(f_r)}{\partial B} = \frac{\varepsilon_r \varepsilon_0 A Q V \omega_r I L}{g^2 k v}. \tag{7}$$

III. LORENTZ-FORCE MEMS MAGNETOMETERS MEASUREMENT: STATE-OF-THE-ART

In the literature there exist a wide variety of strategies to characterize MEMS magnetometers. As a result, it is not always straightforward to translate the reported figures in order to compare the performance of the proposed device with similar works.

The most popular characterization strategy is probably the use of a lock-in amplifier. The use of this instrument varies depending on the work. In [17], [18], [19] the lock-in amplifier is used to put the device in a closed loop, whose voltage and current biasing references are generated by the instrument as well as to demodulate the signal. The measurement setup is similar in [20], [21], [22] with the difference that no voltage driving is used. Next, [5], [23] use the lock-in amplifier only to demodulate the output of the sensor, as the current reference is generated by an oscillator. Finally, the works in [24], [25] use the lock-in amplifier to close the loop and generate the voltage driving, but not the current biasing, which is performed at DC as a result of a different device design approach: the device under test does not use capacitive readout but thermal-piezoresistive amplification. The main disadvantage of using a lock-in amplifier is the need of an amplification circuit to interface the device with the instrument, as well as to translate the lock-in amplifier output to the desired biasing. As a result, custom circuits are needed for each device, making it difficult to reuse them. Furthermore, in such works the device sensitivity is provided in units of voltage over Tesla V/T, sometimes without disclosing the amplifier gain nor the circuit parameters, making it difficult to know the final figures of the standalone device.

The Vector Network Analyzer (VNA) is also a popular instrument used to characterize Lorentz-force MEMS magnetometers. The VNA provides information on the spectrum of the output signal and it is sometimes used as a reference to generate some [26] or all the biasing [27], [28] in some

sort of closed loop. In [29] the VNA is only used to characterize the device resonance, while a spectrum analyzer is used to obtain the sensitivity when the device is driven with a waveform generator. In this case, unfortunately, interfacing amplifiers are still needed. Moreover, the device characterization is usually given in units of V/T, from the interface circuit, and dB, from the VNA.

Laser Doppler Vibrometers (LDV) are generally used in works where the characterization of the mechanical performance of the device is disclosed, as it provides information on the rotor displacement in units of meters [30], [31], [32], [33]. This instrument, though, is usually combined with other strategies that provide electrical characterization: in [30], a LDV is combined with a differential amplifier that provides a capacitive sensing characterization, and [32] combines the LDV with a VNA. The work in [33] deserves a special mention, as it uses a lock-in amplifier to filter the noisy LVD output. Moreover, it uses two capacitive readout circuits followed by two lock-in amplifiers to read out the device output and generate its biasing.

The spectrum analyzer is another of the instruments that has been used in the literature of Lorentz-force MEMS magnetometers [29], [34], [35], [36]. In [34] a processing electronic circuit is followed by such instrument, and a similar approach is followed in [35], where a function generator is used to perform the biasing. In [36] the spectrum analyzer is used to perform a frequency sweep around the device resonance. Its output is used to generate the reference for a Howland current source that creates the device current biasing. Again, the device sensitivity is usually given in V/T units.

Finally, it is worth to mention [37], where a custom readout circuit is used to interface the device with an oscilloscope, and [38], where a commercial capacitive to digital converter chip is used.

IV. PROPOSED MEASUREMENT SYSTEM

The proposed testing setup is based around an impedance analyzer for various reasons: availability in laboratories doing research on MEMS devices, ease of use and steep learning curve, and the convenient measurement and data processing automation by using scripts. Most importantly, though, is the fact that an impedance analyzer allows the characterization of standalone devices in electrical units directly related to the device: capacitance change under a DC voltage sweep (commonly known as C-V curve), and resonance measurement in conductance (G) and susceptance (B) or impedance (Z) [10], [11], [13], [39]. From such measurements, together with the device geometry information, other parameters can be derived, such as gap (g) and gap variation (A_z), quality factor (Q), device output current (i_s), and sensitivity in different units (as shown in Section II) to name some. The proposed testing setup has already been successfully used to characterize Lorentz-force magnetometers [13], [40].

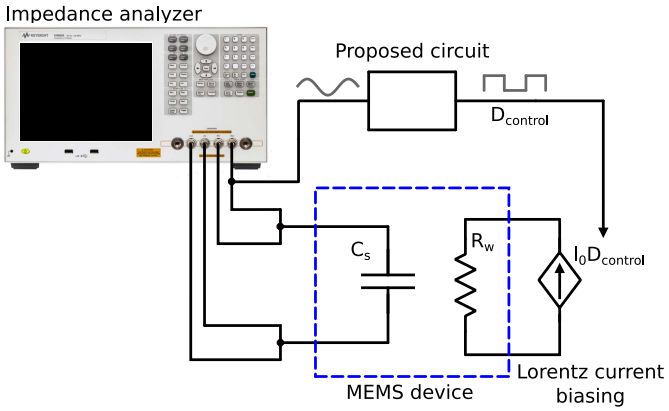

FIGURE 2. Proposed characterization setup for Lorentz force MEMS magnetometers.

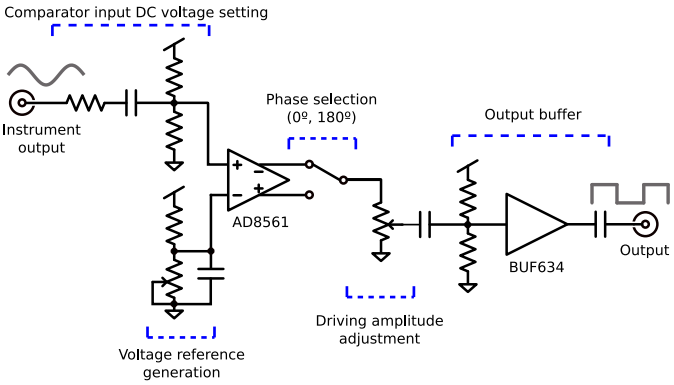

FIGURE 3. Schematic of the proposed circuit to drive the MEMS magnetometer.

The Keysight 4990A (Keysight Technologies, Santa Rosa, CA, USA) impedance analyzer, has been used to characterize the capacitive output of the Lorentz-force magnetometer. The instrument performs 4-wire measurements by driving the device with DC and AC voltages that can be selected by the user. These have been used to generate the v and V in the equations derived in Section II. From these four outputs, it has been observed that, from the two ports driving voltage, there is one that provides a low impedance voltage driving, while the other performs a higher impedance voltage sensing, similar to an oscilloscope input. Given these characteristics, it was observed that the instrument signal driving could be buffered and used as a reference for the Lorentz current driving without affecting the measurement given the capability of the instrument to calibrate the wiring parasitics. Then, the buffered signal is processed by the in-phase driving circuit shown in Figure 2. The detailed schematic is depicted in Figure 3.

The processing circuit works as follows. The impedance analyzer signal is band-pass filtered with a high-pass filter and a DC-blocking capacitor. The latter is used to replace the input DC by the board mid-supply voltage. Next, the signal is compared with the board mid-supply voltage with the AD8561 (Analog Devices, Norwood, MA, USA) [41].

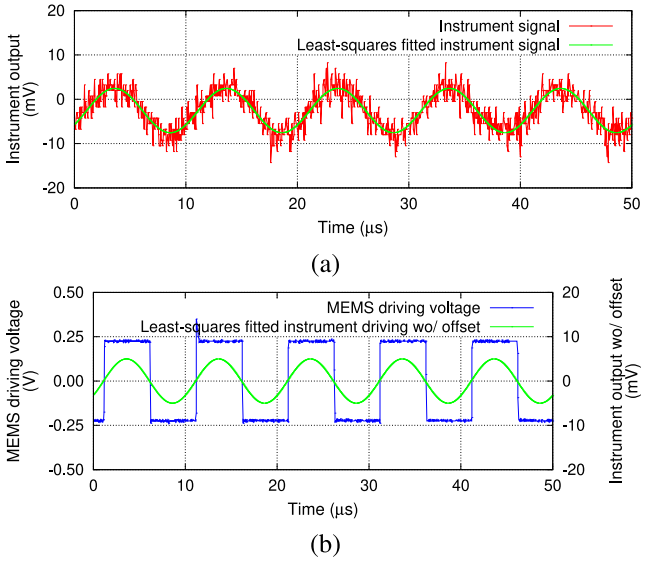

FIGURE 4. In (a) the output signal from the impedance analyzer (in red) and its fitted signal (in green). In (b) the generated driving voltage (in blue) is compared with the offset-less fitted version of the instrument output (in green).

Doing so a square signal in phase with the input voltage is created. Alternatively, the comparator positive output can be fed back to the negative input with a low-pass filter to automatically set the mid-supply operating point. The potentiometer at the comparator negative input is placed in order to allow comparator offset compensation in case it is necessary. Then, the positive and negative outputs of the comparator may be selected with a switch to provide in-phase or 180° signals to the next stage. By default, the in-phase output is selected so that the final Lorentz current is in phase with the impedance analyzer electrostatic driving. The possibility of out-of-phase driving has been implemented as it has the same effect as inverting the sensed magnetic field. Next, a potentiometer is used to adjust the output voltage amplitude, and unity gain buffered with a BUF634 (Texas Instruments, Dallas, TX, USA) [42] to provide good Slew Rate (SR).

V. EXPERIMENTAL VALIDATION

A. STANDALONE VALIDATION

To experimentally validate the proposed circuit, first it has been characterized standalone. Its ability to generate in-phase Lorentz current driving out from very weak input voltage from the instrument has been tested as depicted in Figure 4. Here, a 100 *kHz* low amplitude output voltage from the impedance analyzer, depicted in Figure 4(a), is driven to the proposed circuit. As a result, it generates a driving signal, shown below in 4(b). As it can be seen, even with very weak instrument output voltages, the board can generate a low-noise, fast rising- and falling-edge, output voltage in phase with the input signal. In order to quantify the quality of the generated signal, the output from the impedance analyzer has been fitted to a sinusoidal signal using the least-squares strategy. Then, the offset has been removed and the zero crossings have been compared with the ones in the generated signal, as shown in Figure 4(b). It has been found that the delay of the generated signal compared with the reference one is $t_d = 150 \pm 50\ ns$. The error is obtained by the sampling period of the oscilloscope, which is 50 *ns*. This is equivalent to a phase error of $\varepsilon = 5.4 \pm 1.8°$. Such an error of only 1.5% generates a negligible effect on the device sensitivity. The generated signal is squared, which is not problematic for the device characterization if some considerations are taken into account. A square signal has theoretically infinite odd harmonics. Hence, it must be taken into account that $2n+1$ harmonics have a small but not negligible effect on the total Lorentz force generated on the MEMS rotor. Moreover, given the signal decoupling performed by the comparator, the circuit output signal remains the same when the input voltage driving is changed by the user. Second, the proposed solution working frequency range is measured by loading the circuit with the input of an Agilent N9320A (Agilent Technologies, Santa Clara, CA, USA) spectrum analyzer 50 Ω load with a 100 mV_{rms} amplitude signal. The resulting plot is depicted in Figure 5. The attenuation at lower frequencies is due to high-pass DC-blocking capacitor, while the 1 *dB* peaking before roll-off is due to the buffer frequency response, which can be removed with minor circuit improvements [42]. Nevertheless, the -3 *dB* cutting frequency is around 10 *MHz*, which is half the bandwidth of the impedance analyzer, even though the buffer allows larger bandwidths with minor circuit adjustments [42], but such frequencies were not targeted as the circuit was designed to characterize devices operating at frequencies no higher than 200 *kHz*. Two main limitations, related to the frequency characteristic, can be identified from the proposed circuit. First, a circuit optimization should be performed to allow the characterization of very low frequency devices, as in the current version the DC blocking limits the lower working frequency. Second, the limited driving buffer SR must be taken into account if high current driving is to be performed to high frequency devices. Otherwise, higher harmonics of the Lorentz current may be attenuated, providing a lower sensitivity.

B. VALIDATION BY MEASURING LORENTZ-FORCE MEMS MAGNETOMETERS

Next, the proposed circuit is used to characterize two different CMOS-MEMS Lorentz-force magnetometers: a 2-axis lateral [13], and a Z-axis magnetometer [12]. A picture of the experimental setup for the Z-axis magnetometer is depicted in Figure 6. Coincidentally, the Lorentz wire resistances of the devices are 45 Ω and 4.6 *k*Ω respectively, which allow the verification of the circuit performance for a wide range of loads. For characterization, the MEMS device is placed in a PCB socket connected with coaxial connectors. The board is placed inside a custom Helmholtz coil that generates an adjustable uniform magnetic field. Moreover, in the case of the device in [13] the board and the coil are placed inside a vacuum chamber. The device in [12] is vacuum packaged.

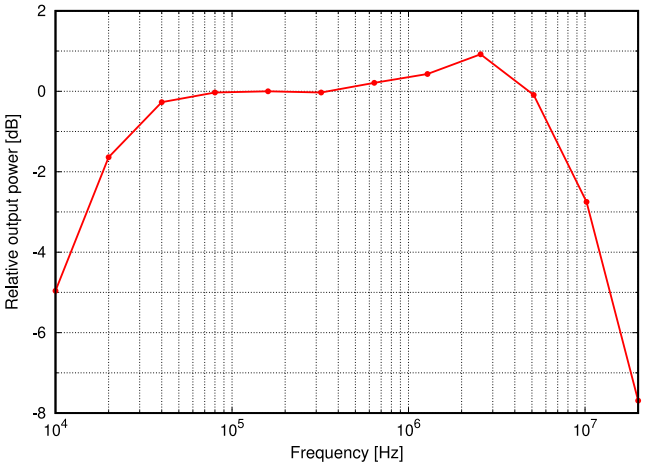

FIGURE 5. Proposed circuit relative output power when driving a 50 Ω with 100 mV_{rms} at 100 *kHz*.

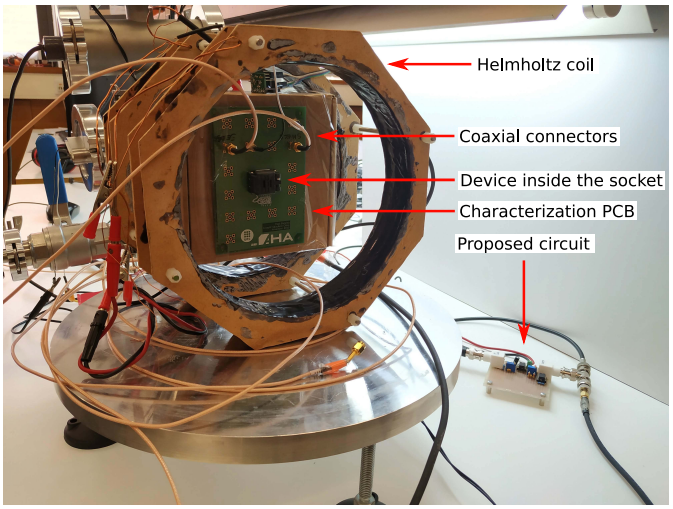

FIGURE 6. Experimental setup for the measurement of MEMS magnetometers using the proposed circuit. The board with the sample is placed inside a custom Helmholtz coil. On the lower right corner, the proposed circuit can be seen.

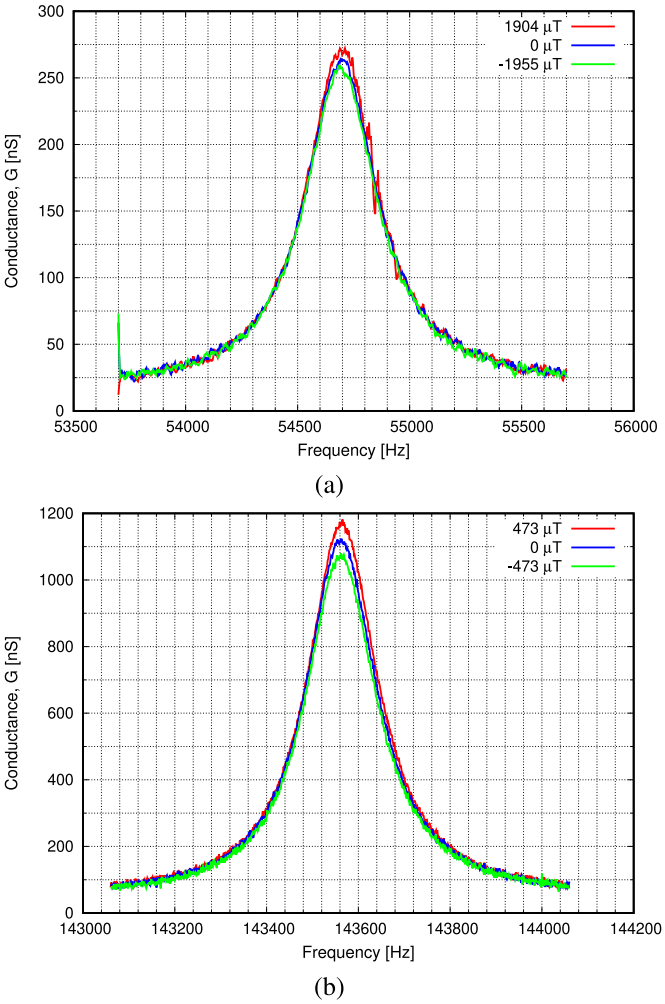

FIGURE 7. Conductance around the mechanical resonance for the lateral (a) and Z-axis (b) CMOS-MEMS magnetometers under the presence of various magnetic fields. The devices have been voltage biased with the impedance analyzer while the injected current is generated with the proposed circuit.

Applying vacuum is done in order to boost the device quality factor and sensitivity, as usually done in this type of devices [20], [22]. The proposed circuit and impedance analyzer are connected as described previously and depicted in Figure 2.

First, conductance (G) for various magnetic fields is measured around the devices' mechanical resonance, where the sensitivity to magnetic field is boosted by the effect of Q and thus, it is easier to distinguish. Measured conductances are shown in Figure 7(a) for the lateral and in Figure 7(b) for the Z-axis device.

Next, these measurements have been performed for various magnetic fields and the conductance values at the resonance frequency have been obtained and used to plot the conductance sensitivity to magnetic field in Figure 8(a) for the lateral and in 8(b) for the Z-axis device, showing the possibility to characterize the devices using the proposed circuit. As in can be seen in such figures, the larger dispersion of values for the lateral axis device is due to its lower Q and Signal-to-Noise Ratio (SNR). The conductance peak for each resonance measurement is obtained with the method explained in [13].

In order to assess that the sensitivity obtained using the proposed circuit is correct, the data from the Z-axis device is compared against the sensitivity obtained in [12]. In that article, the device was amplitude modulated using a self-sustained oscillation, closed-loop circuit that ensures that the device is always driven at its resonance frequency and that total loop phase is 0°. There the sensitivity was measured to be 9.75 $pA/\mu T$ while driving the device with a DC voltage of $V_{DC[12]} = 1\ V$, an AC voltage of $v = 6\ mV_{rms}$ and a Lorentz current of $I_{L[12]} = 300\ \mu A_{rms}$. Contrarily, in this article the parameters used are $V_{DC} = 0.5\ V$, $V_{AC} = 10\ mV_{rms}$, and $I_L = 50\ \mu A_{rms}$ and the sensitivity is 0.103 $nS/\mu T$. Both sensitivity units are equivalent, as it is demonstrated in eq. (6) and (7). In order to allow a comparison, the sensitivity

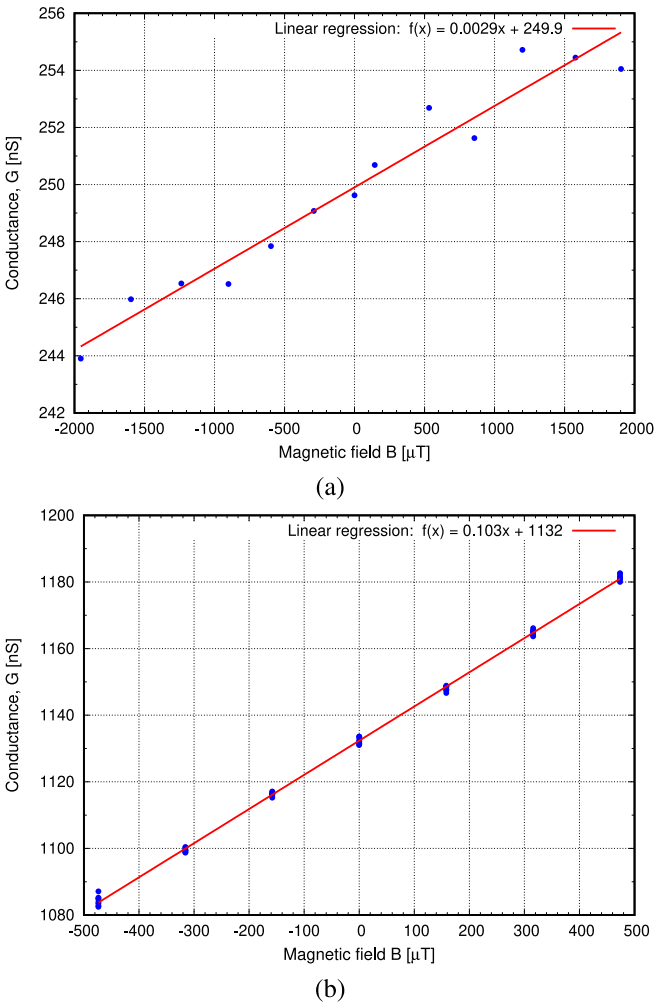

FIGURE 8. Lateral axis (a) and Z-axis (b) devices conductance as a function of magnetic field.

in [12] is converted into $nS/\mu T$ units

$$\begin{aligned} S_{[12]} &= 9.75\frac{pA}{\mu T}\cdot\underbrace{\frac{1\ nA}{1000\ pA}}_{(1)}\cdot\underbrace{\frac{V_{DC}}{V_{DC[12]}}}_{(2)}\cdot\underbrace{\frac{I_L}{I_{L[12]}}}_{(3)}\cdot\underbrace{\frac{1}{v\sqrt{2}}}_{(4)} \\ &= 9.75\frac{pA}{\mu T}\cdot\underbrace{\frac{1\ nA}{1000pA}}_{(1)}\cdot\underbrace{\frac{0.5\ V}{1\ V}}_{(2)}\cdot\underbrace{\frac{50\ \mu A_{rms}}{300\ \mu A_{rms}}}_{(3)}\cdot\underbrace{\frac{1}{v\sqrt{2}}}_{(4)} \\ &= 0.095\ nS/\mu T \end{aligned} \tag{8}$$

where current units are translated from pA to nA in (1), the different DC voltage biasing and Lorentz currents are translated in (2) and (3) respectively, and (4) translates the peak voltage into rms and the AC voltage is included to finally convert units of current into conductance as $S_G(B) = S_{i_s}(B)/v$. Both sensitivities are very similar, demonstration the equivalence of both methods and the correctness of the standalone method proposed in this article. The 7.8% difference between sensitivities is though to be a consequence of the limited bandwidth of the injected current

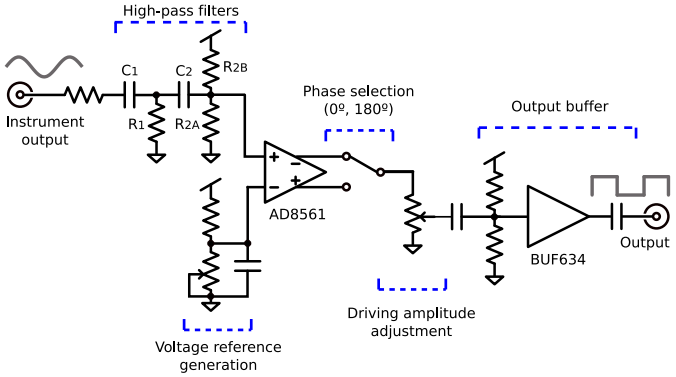

FIGURE 9. Schematic of the proposed circuit for FM operation. Note the high-pass filters at the input providing the required 90° phase shift.

in [12], which is though to limit the Lorentz force higher order harmonics that add up to force at the fundamental frequency

$$F_{Ln} = \frac{4}{\pi}\left(sin(\omega t) + \frac{1}{3}sin(3\omega t) + \frac{1}{5}sin(5\omega t) + \cdots\right) \tag{9}$$

where F_{Ln} is the normalized Lorentz force. If sinusoidal current driving is needed, a quite selective filter should be placed at the buffer output in order to filter out the higher harmonics without attenuating the fundamental component.

VI. OPERATION IN FM

In order to operate the Lorentz-force magnetometer in FM mode [14], the proposed setup can be easily modified to generate a Lorentz current driving in quadrature with the voltage driving of the impedance analyzer.

In order to do so, we can add an additional high-pass filter to the comparator input, as depicted in Figure 9. First-order high-pass filters provide a predictable way to generate a phase shift as a function of the frequency. Their cutoff frequency and phase shift follows the equations:

$$f_c = \frac{1}{2\pi RC} \qquad \Theta = \tan^{-1}\left(\frac{f_c}{f}\right) \tag{10}$$

where f_c is the cutoff frequency of the filter, f is the input frequency and R and C the resistor and capacitor values, respectively. Beware, however, that the input frequency cannot be much smaller than f_c, otherwise it will be heavily attenuated and the comparator will not trigger. If we have two first-order filters in cascade, we can easily obtain a 90° phase shift by making their respective cutoff frequencies equal to the resonant frequency, that is $f_c = f_r$, hence each one providing a phase shift $\Theta = 45°$ and an overall system response in quadrature while only attenuating the voltage in half.

In order to prevent loading effects of the second filter stage on the first one, thus deviating the phase response from the theoretical calculations, it is recommended that $R_{2A}\|R_{2B} > 10\ R_1$ and $C_2 < 10\ C_1$, while keeping the ratios of $R_1/C_1 = R_{2A}\|R_{2B}\ /\ C_2$, otherwise some filter components

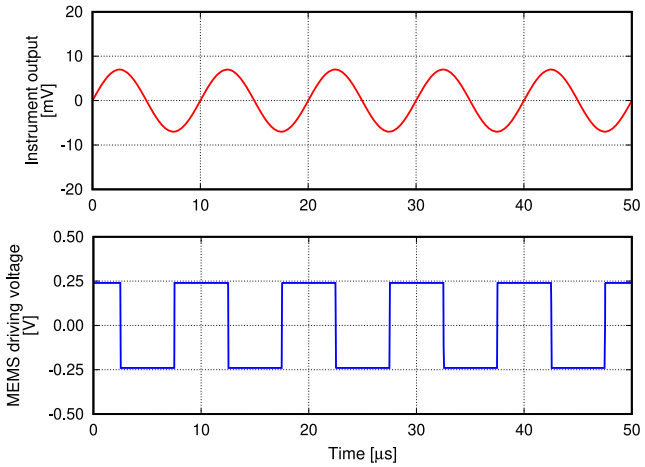

FIGURE 10. Simulation of the proposed setup response for quadrature operation in FM. Output signal from the impedance analyzer is on top (red), and the generated driving voltage is on the bottom (blue). Note the 90° phase shift between the two.

would need to be experimentally adjusted in order to obtain a phase response near 90°. A simulation of the transient response of the setup in FM mode can be seen in Figure 10. The advantage of this solution is its easy implementation requiring only passive components. Unfortunately, it suffers from attenuation and its working frequency range is limited, only useful for devices with a known and stable resonance frequency.

Another alternative for implementing the phase shift for FM operation is using an opamp-based differentiator. Given that the circuit input signal is a sinusoidal wave following $v_i = v\sin(2\pi ft)$, a differentiator would provide at the output

$$v_o = 2\pi fv\cos(2\pi ft) = 2\pi fv\sin\left(2\pi ft - 90^\circ\right) \qquad (11)$$

where v is the input voltage amplitude. The advantage of this circuit over the high-pass filter is the higher output amplitude as well as the capability of working over a larger frequency range. The price to pay, though, is the need of an active circuit that has to be supplied, as well as potential amplifier output saturation due an excessive gain at higher frequencies.

VII. CONCLUSION

In this article, a comprehensive strategy for rapid and accurate characterization of Lorentz-force MEMS magnetometers has been proposed. The objective of the work is an attempt to unify the various strategies found in the literature in order to get easy to compare devices. Due to its availability and ease of use, the proposed circuit is designed around an impedance analyzer. The proposed circuit has been demonstrated to accurately buffer the instrument output voltage and to drive it, in-phase, to the MEMS magnetometer in order to generate the Lorentz current. Doing so, MEMS characterization has been demonstrated when operated under AM operation mode. We have also presented two alternative and simple changes to apply to the proposed circuit that would allow the characterization under FM operation mode. Finally, the proposed circuit has been used in two very different devices, demonstrating the ability to drive Lorentz wires within two different order of magnitude, as well as being capable to be used for devices with resonance frequencies as high as 10 *MHz*.

REFERENCES

[1] "Technology trends for inertial MEMS," Yole Développement, Villeurbanne, France, Rep., Jan. 2012.
[2] "6- & 9-axis sensors consumer inertial combos," Yole Développement, Villeurbanne, France, Rep., Oct. 2014.
[3] "Magnetic sensor. Market and technology report—November 2017," Yole Développement, Villeurbanne, France, Rep., Nov. 2017.
[4] A. Lahrach, "eCompass comparative report: 3-axis & 6-axis eCompass for consumer applications technology and cost review," Syst. Plus Consul., Nantes, France, Rep., Oct. 2015.
[5] C. R. Marra *et al.*, "100 $nT/\sqrt{Hz}$, 0.5 mm^2 monolithic, multi-loop low-power 3-axis MEMS magnetometer," in *Proc. IEEE Micro Electro Mech. Syst. (MEMS)*, Belfast, U.K., 2018, pp. 101–104.
[6] D. Fernández, J. Ricart, and J. Madrenas, "Experiments on the release of CMOS-micromachined metal layers," *J. Sens.*, vol. 2010, pp. 1–7, May 2010. [Online]. Available: https://www.hindawi.com/journals/js/2010/937301/
[7] J. Valle, D. Fernández, O. Gibrat, and J. Madrenas, "Manufacturing issues of BEOL CMOS-MEMS devices," *IEEE Access*, vol. 9, pp. 83149–83162, 2021.
[8] P. Michalik, J. M. Sánchez-Chiva, D. Fernández, and J. Madrenas, "CMOS BEOL-embedded z-axis accelerometer," *Electron. Lett.*, vol. 51, no. 11, pp. 865–867, 2015.
[9] P. Michalik, J. M. Sánchez-Chiva, D. Fernández, and J. Madrenas, "CMOS BEOL-embedded lateral accelerometer," in *Proc. IEEE SENSORS*, Busan, South Korea, 2015, pp. 1–4.
[10] S. Banerji, D. Fernández, and J. Madrenas, "Characterization of CMOS-MEMS resonant pressure sensors," *IEEE Sensors J.*, vol. 17, no. 20, pp. 6653–6661, Oct. 2017.
[11] D. Mata-Hernandez, D. Fernández, S. Banerji, and J. Madrenas, "Resonant MEMS pressure sensor in 180 nm CMOS technology obtained by BEOL isotropic etching," *Sensors*, vol. 20, no. 21, p. 6037, 2020.
[12] J. M. Sánchez-Chiva, J. Valle, D. Fernández, and J. Madrenas, "A mixed-signal control system for Lorentz-force resonant MEMS magnetometers," *IEEE Sensors J.*, vol. 19, no. 17, pp. 7479–7488, Sep. 2019.
[13] J. M. Sánchez-Chiva, J. Valle, D. Fernández, and J. Madrenas, "A CMOS-MEMS BEOL 2-axis Lorentz-force magnetometer with device-level offset cancellation," *Sensors*, vol. 20, no. 20, p. 5899, 2020.
[14] M. Li *et al.*, "Lorentz force magnetometer with quadrature frequency modulation," in *Proc. Solid-State Sens. Actuat. Microsyst. Workshop*, May 2014, pp. 52–55.
[15] S. Sonmezoglu, I. B. Flader, Y. Chen, D. D. Shin, T. W. Kenny, and D. A. Horsley, "Dual-resonator MEMS magnetic sensor with differential amplitude modulation," in *Proc. 19th Int. Conf. Solid-State Sens. Actuat. Microsyst. (TRANSDUCERS)*, Kaohsiung, Taiwan, 2017, pp. 814–817.
[16] S. Sonmezoglu, I. B. Flader, Y. Chen, D. D. Shin, T. W. Kenny, and D. A. Horsley, "Dual-resonator MEMS Lorentz force magnetometer based on differential frequency modulation," in *Proc. IEEE Int. Symp. Inertial Sens. Syst. (INERTIAL)*, Kauai, HI, USA, 2017, pp. 160–163.
[17] M. Li, V. T. Rouf, M. J. Thompson, and D. A. Horsley, "Three-axis Lorentz-force magnetic sensor for electronic compass applications," *J. Microelectromech. Syst.*, vol. 21, no. 4, pp. 1002–1010, Aug. 2012.
[18] V. T. Rouf, M. Li, and D. A. Horsley, "Area-efficient three axis MEMS Lorentz force magnetometer," *IEEE Sensors J.*, vol. 13, no. 11, pp. 4474–4481, Nov. 2013.
[19] Z. Yan, Y. Hao, W. Li, Z. Zhang, and H. Chang, "A mode-localized Lorentz force magnetometer with 1.6 $\mu T/\sqrt{Hz}$ resolution," in *Proc. 20th Int. Conf. Solid-State Sens. Actuat. Microsyst. Eurosens. XXXIII (TRANSDUCERS EUROSENSORS XXXIII)*, Berlin, Germany, 2019, pp. 1815–1818.

[20] G. Langfelder, C. Buffa, A. Frangi, A. Tocchio, E. Lasalandra, and A. Longoni, "Z-axis magnetometers for MEMS inertial measurement units using an industrial process," *IEEE Trans. Ind. Electron.*, vol. 60, no. 9, pp. 3983–3990, Sep. 2013.
[21] S. Dellea *et al.*, "Off-resonance operation of in-plane torsional MEMS magnetometers," *Procedia Eng.*, vol. 87, pp. 819–822, Jan. 2014.
[22] M. Li *et al.*, "Single-structure 3-axis Lorentz force magnetometer with sub-30 $nT/\sqrt{HZ}$ resolution," in *Proc. IEEE 27th Int. Conf. Micro Electro Mech. Syst. (MEMS)*, San Francisco, CA, USA, 2014, pp. 80–83.
[23] C. R. Marra, M. Gadola, G. Laghi, G. Gattere, and G. Langfelder, "Monolithic 3-axis MEMS multi-loop magnetometer: A performance analysis," *J. Microelectromech. Syst.*, vol. 27, no. 4, pp. 748–758, Aug. 2018.
[24] M. Mahdavi, A. Ramezany, V. Kumar, and S. Pourkamali, "SNR improvement in amplitude modulated resonant MEMS sensors via thermal-piezoresistive internal amplification," in *Proc. 28th IEEE Int. Conf. Micro Electro Mech. Syst. (MEMS)*, Estoril, Portugal, 2015, pp. 913–916.
[25] V. Kumar, M. Mahdavi, X. Guo, E. Mehdizadeh, and S. Pourkamali, "Ultra sensitive Lorentz force MEMS magnetometer with pico-tesla limit of detection," in *Proc. 28th IEEE Int. Conf. Micro Electro Mech. Syst. (MEMS)*, Estoril, Portugal, 2015, pp. 204–207.
[26] V. Kumar, A. Ramezany, M. Mahdavi, and S. Pourkamali, "Amplitude modulated Lorentz force MEMS magnetometer with picotesla sensitivity," *J. Micromech. Microeng.*, vol. 26, no. 10, 2016, Art. no. 05021.
[27] E. Mehdizadeh, V. Kumar, and S. Pourkamali, "Sensitivity enhancement of Lorentz force MEMS resonant magnetometers via internal thermal-piezoresistive amplification," *IEEE Electron Device Lett.*, vol. 35, no. 2, pp. 268–270, Feb. 2014.
[28] S. Ghosh and J. E.-Y. Lee, "An ultra-sensitive piezoelectric-on-silicon flapping mode MEMS lateral field magnetometer," in *Proc. Joint Conf. Eur. Freq. Time Forum IEEE Int. Freq. Control Symp. (EFTF/IFCS)*, Besancon, France, 2017, pp. 502–505.
[29] W. L. Sung, F. Y. Lee, C. L. Cheng, C. I. Chang, E. Cheng, and W. Fang, "MEMS above CMOS process for single proof-mass 3-axis Lorentz-force resonant magnetic sensor," in *Proc. IEEE 29th Int. Conf. Micro Electro Mech. Syst. (MEMS)*, Shanghai, China, 2016, pp. 978–981.
[30] M. J. Thompson and D. A. Horsley, "Resonant MEMS magnetometer with capacitive read-out," in *Proc. IEEE SENSORS*, Christchurch, New Zealand, 2009, pp. 992–995.
[31] J. Chen, M. Qin, and Q. A. Huang, "Measurement of the magnitude and direction of magnetic field by a micromachined cantilever," in *Proc. 16th Int. Solid-State Sens. Actuat. Microsyst. Conf.*, Beijing, China, 2011, pp. 1108–1111.
[32] V. Rochus *et al.*, "Poly-SiGe-based MEMS xylophone bar magnetometer," in *Proc. SENSORS*, Taipei, Taiwan, 2012, pp. 1–4.
[33] M. Stifter, F. Keplinger, W. Hortschitz, and T. Sauter, "Principles of nonlinear MEMS-resonators regarding magnetic-field detection and the interaction with a capacitive read-out system," *Microsyst. Technol.*, vol. 20, pp. 783–791, Apr. 2014.
[34] B. Bahreyni and C. Shafai, "A micromachined magnetometer with frequency modulation at the output," in *Proc. IEEE SENSORS*, Irvine, CA, USA, 2005, p. 4.
[35] C. I. Chang, M.-H. Tsai, Y.-C. Liu, C.-M. Sun, and W. Fang, "Development of multi-axes CMOS-MEMS resonant magnetic sensor using Lorentz and electromagnetic forces," in *Proc. IEEE 26th Int. Conf. Micro Electro Mech. Syst. (MEMS)*, Taipei, Taiwan, 2013, pp. 193–196.
[36] G. Langfelder, A. Tocchio, E. Lasalandra, and A. Longoni, "Comparison of Lorentz-force MEMS magnetometers based on different capacitive sensing topologies," in *Proc. Transducers Eurosens. XXVII 17th Int. Conf. Solid-State Sens. Actuat. Microsyst. (TRANSDUCERS EUROSENSORS XXVII)*, Barcelona, Spain, 2013, pp. 709–712.
[37] C.-H. Hsieh, C.-L. Dai, and M.-Z. Yang, "Fabrication and characterization of CMOS-MEMS magnetic microsensors," *MDPI Sens.*, vol. 13, pp. 14728–14739, Nov. 2013.
[38] M. Y. Elsayed, P.-V. Cicek, F. Nabki, and M. N. El-Gamal, "Surface micromachined combined magnetometer/accelerometer for above-IC integration," *J. Microelectromech. Syst.*, vol. 24, no. 4, pp. 1029–1037, Aug. 2015.
[39] P. Michalik, D. Fernández, M. Wietstruck, M. Kaynak, and J. Madrenas, "Experiments on MEMS integration in 0.25μm CMOS process," *MDPI Sens.*, vol. 18, no. 7, p. 2111, 2018.
[40] J. M. Sánchez-Chiva, D. Fernández, and J. Madrenas, "A test setup for the characterization of Lorentz-force MEMS magnetometers," in *Proc. 27th IEEE Int. Conf. Electron. Circuits Syst. (ICECS)*, Glasgow, U.K., 2020, pp. 1–4.
[41] *Ultrafast 7 ns Single Supply Comparator, Rev. D*, Analog Devices, Norwood, MA, USA, 2016.
[42] *BUF634 250-mA High-Speed Buffer, Rev. B*, Texas Instrum., Dallas, TX, USA, 2019.

JOSEP MARIA SÁNCHEZ-CHIVA was born in Barcelona, Spain, in 1989. He received the B.Sc. degree in telecommunication engineering, the M.Sc. degree in electronic engineering, and the Ph.D. degree in electronic engineering from the Universitat Politècnica de Catalunya, Barcelona, in 2011, 2014, and 2020, respectively. During his thesis, he designed CMOS-MEMS Lorentz-force magnetometers and the readout circuits and systems. From 2012 to 2013, he was an Analog Design Intern with Broadcom, Barcelona, in the field of Sigma-Delta ADC's. From 2018 to 2020, he worked as a ASIC Design Engineer with Nanusens, Cerdanyola del Vallès, Spain, where he designed circuits for the signal readout of monolithic CMOS-MEMS accelerometers. He is currently a Postdoctoral Researcher with the LIP6, Sorbonne Université, Paris, France, where he develops integrated power management circuits for remote powered implants.

JUAN VALLE was born in Lugo, Spain, in 1977. He received the first M.Sc. degree in physics and the second M.Sc. degree in industrial engineering from Universidad Alfonso X El Sabio, Madrid, Spain, in 2000 and 2002, respectively. He is currently pursuing the Ph.D. degree in electronic engineering with the Universitat Politécnica de Catalunya (UPC), Barcelona, Spain. From 2001 to 2002, he worked as a Microsystems (MEMS) and Nanotechnology Consultant with the National Institute for Aerospace Technology. He is currently a Senior MEMS Development Engineer with SiTime, while he is finishing his Ph.D. in electronic engineering with UPC. He specialized on multiphysics simulations before joining Delphi Diesel Systems, U.K., as an Analyst Engineer in 2004, and joined Baolab Microsystems in 2005, where he researched on the fields of MEMS sensors and micromanufacturing processes for nine years, where he filled ten patent applications on related fields. He devised design techniques applicable for the MEMS fabrication inside the CMOS BEOL. Using these techniques, the first CMOS-MEMS three axis magnetometer aimed at mass production was developed.

DANIEL FERNÁNDEZ received the Ph.D. degree in microelectronics (*cum laude*) and the M.B.A. degree from Universitat Politècnica de Catalunya (UPC), Barcelona, Spain, in 2008 and 2009, respectively, where he worked as a Postdoctoral Researcher with the Electronic Engineering Department, from 2008 to 2010, in the fields of CMOS surface micromachining, circuits and control architectures for MEMS sensors and actuators, translinear circuits for analog signal processing and the design of integrated power converters. From 2010 to 2014, he worked as a Principal ASIC Engineer with Baolab Microsystems developing circuits and architectures for CMOS MEMS/NEMS-based products, and as a ASIC Design Engineer Contractor for the European Space Agency designing radiation-hardened integrated circuits and interface blocks for space exploration in interplanetary missions. In 2014, he co-founded Nanusens, a deep-tech start-up company dedicated to CMOS-MEMS design, and he served as its Chief Technology and Science Officer by developing circuits and architectures for MEMS sensors signal conditioning, leading teams up to seven researchers and several subcontracted companies, and managing R&D projects up to 3 M€ budgets. Since 2020, he has been a Senior Researcher Engineer with the Institut de Física d'Altes Energies (IFAE-BIST), where he develops innovative integrated circuits for medical implants.

JORDI MADRENAS received the M.Sc. degree in Telecommunication Engineering and the Ph.D. degree from the Universitat Politècnica de Catalunya (UPC), Barcelona, Spain, in 1986 and 1991, respectively, where he is a Professor with the Electronics Engineering Department. He coordinates the Integrated Smart Sensors and Health Technologies (ISSET) Research Group. From 2000 to 2003, he was the Vice Dean of Studies with the Telecommunication Engineering School of Barcelona, UPC. He has participated in five European projects and has coordinated six Spanish national research projects and several contracts with companies. He currently leads a national project on microelectromechanical systems (MEMS) on-chip and microsensor bioinspired signal processing. He has coauthored 45 scientific journals, 140 international conference papers, two books, six book chapters, and holds one international patent. His current research interests include analog, mixed-signal and digital VLSI and FPGA design, CMOS-MEMS design and conditioning, ultra-low-power design, and bioinspired/neuromorphic system implementation.